geodl: An R package for geospatial deep learning semantic segmentation using torch and terra

Aaron E. Maxwell*, West Virginia University Department of Geology and Geography, Brooks Hall, Morgantown, WV 26506. Aaron.Maxwell@mail.wvu.edu

Sarah Farhadpour, West Virginia University Department of Geology and Geography, Brooks Hall, Morgantown, WV 26506. sf00039@mix.wvu.edu

Srinjoy Das, West Virginia University School of Mathematical and Data Sciences, Armstrong Hall, Morgantown, WV 26506. srinjoy.das@mail.wvu.edu.

*Corresponding author

Paper is a non-peer reviewed preprint submitted to *EarthArXiv*.

The paper has been submitted for peer review to the journal *PLOS ONE*.

Abstract

Convolutional neural network (CNN)-based deep learning (DL) methods have transformed the analysis of geospatial, Earth observation, and geophysical data due to their ability to model spatial context information at multiple scales. Such methods are especially applicable to pixel-level classification, or semantic segmentation, tasks. A variety of R packages have been developed for processing and analyzing geospatial data. However, there are currently no packages available for implementing geospatial DL in the R language and data science environment. This paper introduces the geodl R package, which supports pixel-level classification applied to a wide range of geospatial or Earth science data that can be represented as multidimensional arrays where each channel or band holds a predictor variable. geodl is built on the torch package, which supports the implementation of DL using the R and C++ languages without the need for installing a Python/PyTorch environment. This greatly simplifies the software environment needed to implement DL in R. Using geodl, geospatial raster-based data with varying numbers of bands, spatial resolutions, and coordinate reference systems are read and processed using the terra package, which makes use of C++ and allows for processing raster grids that are too large to fit into memory. Training loops are implemented with the luz package. The geodl package provides utility functions for creating raster masks or labels from vector-based geospatial data and image chips and associated masks from larger files and extents. It also defines a torch dataset subclass for geospatial data for use with torch data loaders. UNet-based models are provided with a variety of optional ancillary modules or modifications. Common assessment metrics (i.e., overall accuracy, class-level recalls or producer's accuracies, class-level precisions or user's accuracies, and class-level F1-scores) are implemented along with a modified version of the unified focal loss framework, which allows for defining a variety of loss metrics using one consistent implementation and set of hyperparameters. Users can assess models using standard geospatial and remote sensing metrics and methods and use trained models to predict to large spatial extents.

Introduction

Need and justification

Pixel-level classification, also referred to as semantic segmentation within the computer vision community, has many applications in the geospatial sciences including land cover, forest type, and agricultural mapping. It is also used for differentiation of a class or feature of interest, such as buildings, ships, or landslides, from the surrounding landscape or background [1–3]. Such mapping or modeling tasks commonly rely on supervised learning, where predictor variables and pixel-level labels are used to train an algorithm to generate a model that can then be applied to new geographic extents to generate wall-to-wall predictions or maps. These methods employ geospatial data, structured as multidimensional arrays or data cubes. Representing geospatial data in a consistent multidimensional array format allows the use of a common supervised learning framework [4–6]. Data that can be represented in this format are collected from a variety of platforms (e.g., satellites, aircraft, or drones) and at a wide range of spatial and temporal resolutions. Further, a variety of data types can be represented as multidimensional arrays including true color, color infrared (CIR), multispectral, and hyperspectral imagery and synthetic aperture radar (SAR) backscatter. Additional predictor variables can be derived from individual images (e.g., band indices or principal components) or a timeseries of images (e.g., seasonal medians or coefficients generated from harmonic regression analysis). Other data sources include historic maps and other cartographic representations, land surface parameters (e.g., slope, topographic position index (TPI), topographic roughness index (TRI), and hillshades) derived from digital terrain models (DTMs), derivatives of light detection and ranging (lidar) point clouds (e.g., canopy height models (CHMs) and return intensity images), and subsurface geophysical measurements.

Semantic segmentation via supervised learning that relies purely on convolutional neural network (CNN)-based deep learning (DL) architectures were first introduced in 2014-2015 [7]. Such methods have been shown to be especially powerful due to their ability to use large amounts of labeled data in order to capture spatial context information at varying spatial scales and perform automatic feature extraction for classification tasks [8]. As a result, CNN-based methods are now replacing more established machine learning (ML) algorithms (e.g., support vector machines (SVMs), random forest (RF), and boosted decision trees (BDTs)) which have been traditionally used to label individual pixels or objects derived using geographic object-based image analysis (GEOBIA). CNN-based semantic segmentation has been operationalized and integrated into commercial geospatial software, including ArcGIS Pro [9] via the Image Analyst Extension [10] and ENVI [11] via the Deep Learning Module [12].

Open-source software, data science tools, and datasets have had a positive impact on how science is conducted, and the development of new tools and techniques has hastened the speed of scientific innovation and the transition of knowledge to action while also fostering reproducible and transparent research [13,14]. Open-source software and datasets, application programming interfaces (APIs), modules, and code libraries have reduced cost, increased the accessibility of research tools, and become key components of research and training infrastructure. Open-source DL tools (i.e., code to support data preparation; model creation, training, and validation; and inference to new data) are currently well developed in the Python [15] language and data science environment, resulting from the development of libraries including Tensorflow [16], Keras [17], and PyTorch [18]. This can be partially attributed to the development of DL amongst the computer vision research community, wherein Python is more popular than other common data science environments [19]. However, many data, geospatial, and Earth scientists use R [20], which was

originally developed for statistical computing, data wrangling, and data analysis. This flexible environment offers a large number of specialized packages, familiarity and ease of use, quality of documentation, a large user base, and available integrated development environments (IDEs), such as RStudio [22]. Specialized R packages include those targeted for machine learning tasks such as clustering (e.g., dtwclust [23]) as well as those used for data wrangling (e.g., tidyverse [24]).

A large set of R packages have already been developed for reading, working with, and analyzing geospatial data specifically, such as sf [25], terra [26], star [27], and tmap [28]. The recent release of the terra package, which replaced the raster package [29] and currently (in early 2024) has had over six million downloads from the Comprehensive R Archive Network (CRAN) since its release in March 2020 based on download statistics obtained using the dlstats package [30], has improved computational efficiency for processing large raster grids, including digital elevation data and multispectral imagery [26]. Using the C++ language [31] via the rcpp package [32], terra allows for reading in portions of large raster grids from disk as opposed to reading the entire dataset to memory, which has greatly improved the practical application of raster-based geospatial data handling and analysis in R [26].

Many DL tools in R rely on Python and act as a wrapper for Python libraries. Using the reticulate package [33], R packages such as keras [34], tensorflow [35], and fastai [36] allow for the execution of Python-based DL from the R environment using R code, and therefore requires the installation of Python environments and libraries. Highlighting the interest in implementing DL in R, the keras package has had over two million downloads from CRAN since its release in July 2017. The recently released torch package [37], which is written in R and C++ and built directly on libtorch (the PyTorch C++ backend) [38], simplifies the software stack by eliminating the need for the Python "middleman", thus avoiding reliance on Python and the associated issues stemming from incorrect versions of software or libraries and complications in setting up analytical environments, as well as the difficulties with troubleshooting errors. This is a large step forward in developing a DL experimentation environment and ecosystem native to R and C++. The torch package has been downloaded from CRAN over 160,000 times since its release in August 2020. We argue that there will be increased use of torch as an ecosystem of packages develops around it, as has occurred for the Python-based PyTorch implementation.

Currently, there are no R packages available specifically for DL applied to raster-based geospatial and Earth science data. This is problematic, as there are many demands and issues specific to geospatial and Earth science data, including the need to make use of raster data with varying numbers of channels or bands, maintain map coordinate reference information, assess models using discipline-specific methods and metrics, and merge results to generate map products over large spatial extents. We argue that the torch and terra packages provide a unique framework to implement geospatial semantic segmentation in the R language and data science environment. The torch package provides an R/C++ implementation of DL that does not require Python/PyTorch while terra provides efficient handling and processing of large geospatial raster grids that may not fit into memory.

In this paper, we introduce the geodl package, which builds on torch and terra to support a general supervised learning, CNN-based semantic segmentation DL workflow that can be applied to a variety of geospatial data types structured in multidimensional arrays to characterize two-dimensional patterns to support pixel-level classification tasks. It fills a key gap in the R environment and can ease the adoption of DL by geospatial scientists who have adopted R for research and applied mapping and modeling tasks. It provides utility functions to create raster masks from vector geospatial data, generate image chips from larger raster grids and associated

masks, and collate image chip names and paths into R data frames; implements a generalized UNet-based framework with options to include a variety of ancillary modules; interfaces with the luz package to train models using loss metrics appropriate when class proportions are imbalanced and/or when difficult-to-predict samples should be prioritized; supports assessment of models using standard remote sensing methods and metrics; and allows for trained models to be applied to new data to generate map output. This article describes the package design philosophy and its associated functions and workflow. It also provides example case studies.

Example code and data

Example code and the data required to implement them have been provided via FigShare [39]: https://figshare.com/articles/dataset/geodl_example_data/23835165. Table 1 below lists the provided script files and their associated uses. The provided scripts and the associated data are also described in a README file provided with the repository. More general torch examples are provided on the torch website: https://torch.mlverse.org/. The geodl package source code is available on GitHub: https://github.com/maxwell-geospatial/geodl. It can be downloaded using the remotes package [40]. At the time of this writing, the developers are working towards submitting the package to CRAN.

Table 1. Script files provided for experimentation with the geodl package.

File	Description
accAssessmentExamples.R	Calculation of accuracy assessment metrics at point locations and from raster predictions and raster labels
classificationExampleLCAI.R	Complete workflow for classification of landcover.ai dataset
classificationExampleTopoDL.R	Complete workflow for classification of topoDL dataset
dataPrepExamples.R	Data prep examples including generating masks, image chips, and land surface parameters from digital terrain models
dataSetLoadExamples.R	Define and use dataset and data loaders
luzMetricsExamples.R	Calculate assessment metrics from predictions and labels
spatialPredictionExample.R	Use a trained model to create a prediction of an entire spatial extent
unifiedFocalLossExamples.R	Configuration and calculation of loss metrics

In the provided examples and in this paper we make use of two datasets: topoDL and landcover.ai. The topoDL dataset was created by some of the authors of this paper and represents a binary semantic segmentation problem. Disturbance associated with surface coal mining is denoted on topographic maps with a brown or pink pattern. The topoDL dataset was developed to explore the use of semantic segmentation DL to extract the extents of historic surface mining from topographic maps [41]. The dataset consists of 123 United States (U.S.), 1:24,000-scale, 7.5-minute topographic maps covering parts of eastern Kentucky, 23 covering parts of eastern Ohio, and 25 covering parts of southwestern Virginia. Mine extent masks were derived from the prospect- and mine-related features from U.S. Geological Survey 7.5- and 15-minute topographic quadrangle (version 10.0) dataset [42] generated by the USGS with some additional editing performed by the researchers. Only 7.5-minute maps were used in the dataset. From the provided topographic maps and vector-based mine extent masks, it is possible to generate a large number of

chips to train a DL model, as will be demonstrated in the provided code examples. These data are available on FigShare [39,43].

The Land Cover from Aerial Imagery, or landcover.ai, dataset [44] represents a multiclass classification problem in which five classes are differentiated: background, building, woodland, water, and road. "Wall-to-wall" pixel-level masks or labels were manually generated by the data originators using true color orthophotographs. Of the available photos, 33 have a spatial resolution of 25 cm, while eight have a resolution of 50 cm. A total area of 216.27 km^2 is mapped across different regions in Poland. These image extents can be divided into image chips and associated pixel-level masks using a Python script provided by the data originators. These data can be downloaded from the following website: https://landcover.ai.linuxpolska.com/.

Implementation

Design philosophy

Fig 1 provides an overview of the geodl workflow. Functions prefixed with torch:: are from the torch package while those prefixed with luz:: are from the luz package. Functions with a green check mark indicate those that are used as checks during the workflow or to assess trained models. Diamonds indicate outputs or results: the trained model and predictions to new raster data. In combination with torch, terra, and luz, geodl provides a complete workflow for undertaking geospatial semantic segmentation. Users can employ open source GIS software, such as QGIS [45], to incorporate training data into this workflow and/or preprocess geospatial data.

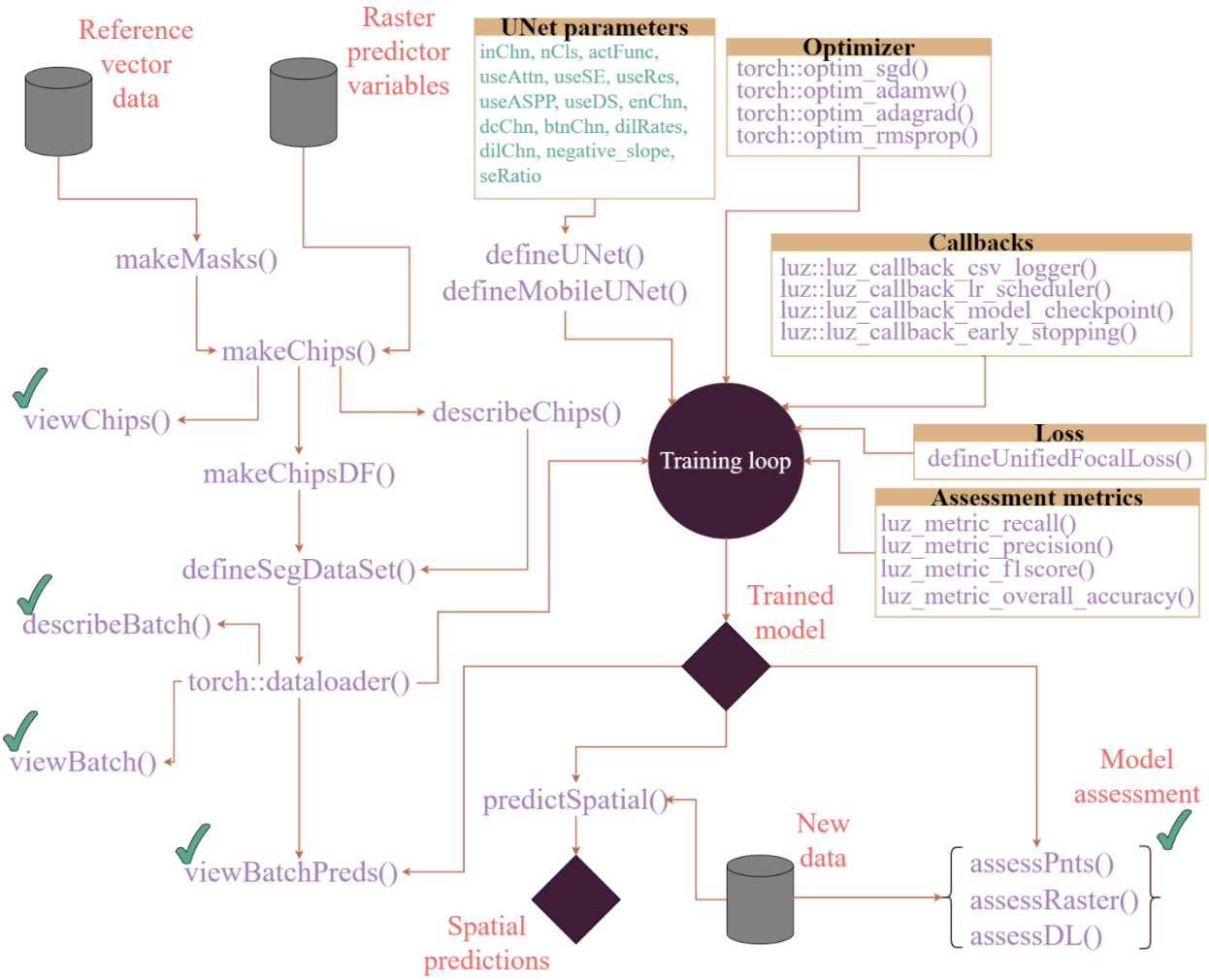

Fig 1. Conceptualization of geodl DL semantic segmentation workflow.

Table 2 lists the package dependencies of geodl and their associated uses. As noted above, the torch package makes use of the libtorch C++ backend as opposed to PyTorch, so there is no need to install a Python environment, in contrast to other DL implementations in R. The terra package is used to read and generally handle raster geospatial data. Spatial reference information is maintained throughout the workflow, and raster grids with varying numbers of channels or bands can be efficiently read and processed. The luz package [46] simplifies the DL training loop, provides implementations of common callbacks (e.g., loggers, model checkpoints, learning rate modifiers, and early stopping), and allows for defining custom loss metrics that can be monitored and aggregated over mini-batches during the training process. It also simplifies the placement and transfer of models and data between the central processing unit (CPU) and graphics processing unit (GPU). The torchvision package [47] provides additional functionality to complement torch for processing image data including applying image augmentations and implementing common computer vision architectures, such as the MobileNet-v2 architecture [48] used within geodl. The dplyr package [49], a key component of the tidyverse [24], is used for general data wrangling, manipulation, and summarization while sf [25] is used to read and process vector geospatial data. The MultiscaleDTM package [50] is used to define custom moving windows for calculating land

surface parameters (LSPs) from digital terrain models (DTMs) within geodl's *makeTerrainDerivatives()* function while psych [51] is used for calculating summary statistics.

Table 2. geodl package dependencies and uses.

Dependency	Use	Reference
torch	Implement DL, tensor manipulations, computational graphs, neural network modules, and optimization algorithms	[37]
terra	Handle geospatial raster data	[26]
luz	Simplify training process, provide callbacks, implement assessment metrics, and handle transfer and placement of data on CPU and GPU	[46]
torchvision	Provide additional functionality for handling and processing image data with torch and apply data augmentations	[47]
dplyr	Generally wrangle, manipulate, and summarize data tables	[49]
sf	Process vector geospatial data	[25]
MultiscaleDTM	Generate moving windows of variable sizes and shapes for digital terrain analysis	[50]
psych	Calculate summary metrics	[51]

The DL workflow as implemented in open-source environments, such as PyTorch, is complicated by inconsistent data representations, dimensionality, and/or data types due to different developers using different conventions. For example, some loss functions require labels to be provided in a 32-bit float data type while others require a long integer data type. Single band, raster-based predictor variables can be represented as two- or three-dimensional arrays: [Width, Height] vs. [Channels/Predictors, Width, Height]. Similarly, associated labels can be stored with a [Class Indices, Width, Height] configuration or a [Width, Height] configuration. The geodl package takes an opinionated stance on defining data dimensionality and types in order to simplify the DL process. The package adheres to the following standards:

1. When using the implemented models, loss metrics, and/or inference tools, data must be provided with the following required shapes and data types. All predictor variable tensors are expected to have a shape of [Channels/Predictors, Width, Height], even if only one predictor variable is provided, and to have a 32-bit float data type. All targets or labels are expected to have a shape of [Class Indices, Width, Height] and a long integer data type. Thus, the channel/predictor or class indices dimension is always included. Once a torch data loader is used to create mini-batches, the shape for each mini-batch will be [Mini-Batch Sample, Channels/Predictors, Width, Height] and the shape of the labels or masks will be [Mini-Batch Sample, Channel Indices, Width, Height].
2. All cases are treated as multiclass classification problems, even when only two classes are differentiated. This means that both positive and background logits are returned and logits are rescaled using a softmax as opposed to sigmoid activation for binary classification

tasks. This design decision was made to standardize and simplify the implementation of losses and assessment metrics.

3. Class indices can start at zero or one. However, no integer values can be skipped. Since R begins indexing at one and due to the use of one-hot encoding in some components of the package, zero index values can cause errors. As a result, sometimes it is necessary to adjust indices such that they start at one. This is the purpose of the *zeroStart* parameter used in many of the implemented functions.

Data preparation and utilities

Creating masks and image chips

It is common for reference labels to be generated as geospatial vector data with point, line, or polygon geometries and stored within a geospatial vector data format, such as a feature class within a file geodatabase, a shapefile, or a layer within a GeoPackage. As a result, it is necessary to provide utilities to convert vector data into categorical or integer raster grids where unique indices differentiate each class or the class of interest and the background. The *makeMasks()* function serves this purpose within geodl; it generates raster masks that align with the available raster predictor variables (i.e., have the same coordinate reference system, spatial resolution, origin, extent, and number of rows and columns of cells). It can also crop predictor variable raster grids and generated masks to a defined extent, as defined by a vector-based polygon boundary. A column in the vector layer attribute table is used to define the class codes, which should start at zero or one and not skip any values (i.e., class codes should be zero to *n* minus one or one to *n* where *n* represents the number of unique categories). For binary classification problems, the background class should be coded as zero and the presence or positive class should be coded as one.

The training and inference processes require that larger raster extents be partitioned into image extents of a defined size (e.g., 128-by-128, 256-by-256, or 512-by-512 cells). These partitions are generally referred to as chips. Each generated chip consists of all the predictor variables as a stack of channels or bands and has a separate mask file with the same number of rows and columns and spatial extent stored as a single channel containing class indices. The *makeChips()* and *makeChipsMultiClass()* functions are used to generate these chips. The *makeChips()* function is used for binary classification problems where the positive class is assigned a value of one and the background class is assigned a value of zero. When more than two classes are differentiated using unique numeric codes, the *makeChipsMultiClass()* function should be used. If the data are sparsely labeled (i.e., not all pixels have class labels even though they belong to a specific class), these pixels should be assigned a unique numeric code that can then be flagged in the loss and/or assessment metric(s) to be assigned a weight of zero, and thus ignored. When using *makeChips()*, all chips can be generated, just those containing at least one pixel mapped to the positive case, or both background-only and positive case chips, which are written to separate folders. This allows the user to control whether all background-only chips are used in the training and/or validation process, or whether only a subset of background-only chips are used. If a chip is incomplete or has null values, generally resulting from a non-rectangular raster extent, that chip will not be written to disk; only complete chips are produced. Chips are written in a TIFF file format. Predictor variable chips are written to an image folder in the selected directory while masks are written to a mask folder within the same directory. If the user specifies that positive and background-only chips should be differentiated, separate positive and background folders are generated in the image and mask folders.

Once chips and associated masks are written to disk, the *makeChipsDF()* function is used to list the names of each chip and associated mask into an R data frame and, optionally, a comma-separated values (CSV) file written to disk. If positive and background-only chips are differentiated, a column is added to the data frame to denote this, which the user can use to filter or subsample the available chips. The *viewChips()* function plots a random set of chips and associated masks from the specified directory and serves as a check. Fig 2 and Fig 3 provide example outputs from this function for the topoDL and landcover.ai datasets, respectively. In order to apply normalization and/or estimate the relative proportion of classes within the dataset, which can be useful for applying class weightings within loss metrics, statistics must be calculated from the chips and associated masks. This is the purpose of the *describeChips()* function. Since a folder may include a large number of chips and/or a chip may contain a large number of pixels, it is possible to calculate statistics from a subsample of chips and/or a subsample of pixels from each chip.

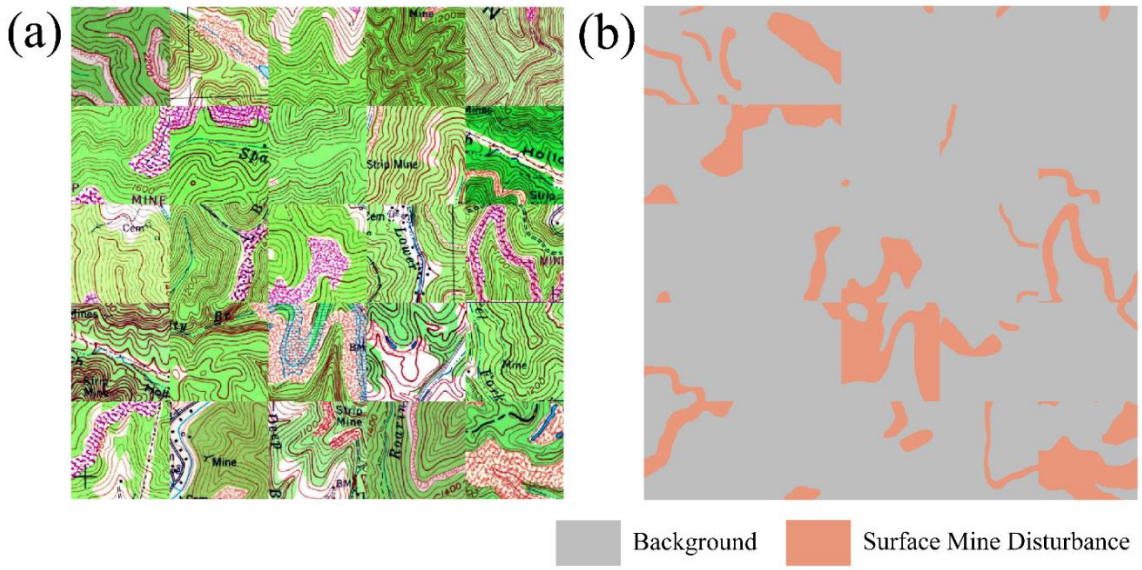

Fig 2. Output from *viewChips()* function for surface mine disturbance extraction from topographic maps using topoDL dataset [43]. (a) image chips; (b) reference masks.

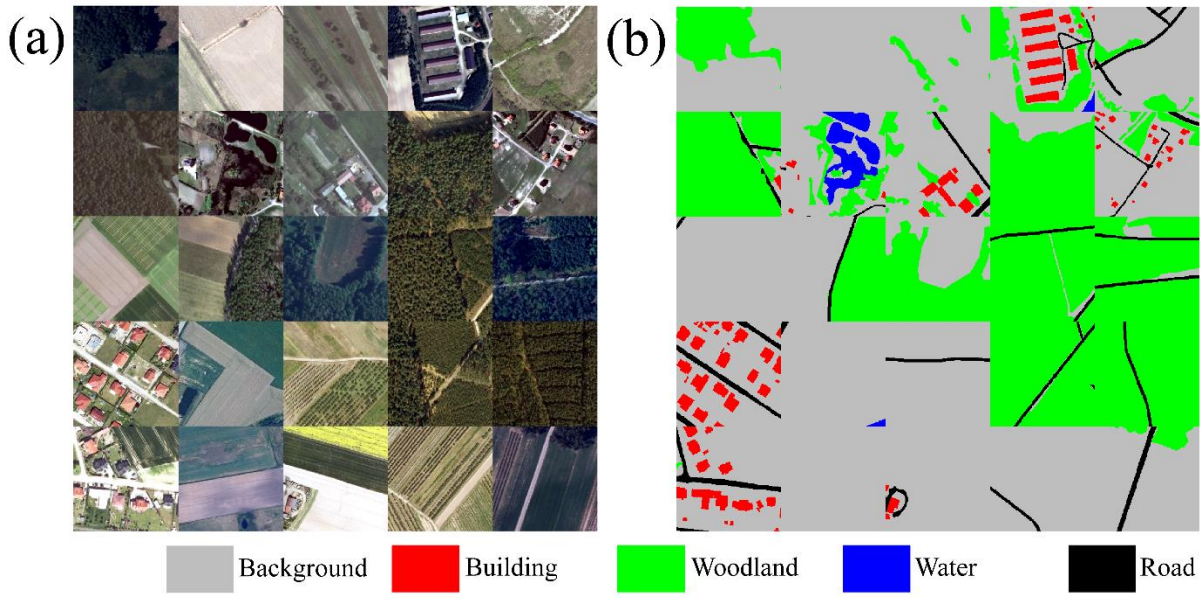

Fig 3. Output from *viewChips()* function for general land cover mapping from landcover.ai dataset [44]. (a) image chips; (b) reference masks.

The *makeTerrainDerivatives()* function creates a three-band raster stack from an input DTM using the method developed by Drs. William Odom and Daniel Doctor of the United States Geological Survey (USGS) and described in Maxwell et al. (2023). This terrain representation can be used as an input feature space for extracting geomorphic or landform features. The first band is a topographic position index (TPI) calculated using a moving window with a 50 m circular radius. The second band is the square root of slope calculated in degrees. The third band is a TPI calculated using an annulus moving window with an inner radius of two meters and an outer radius of five meters. The TPI values are clamped to a range of negative ten to ten then linearly rescaled from zero to one. The square root of slope is clamped to a range of zero to ten then linearly rescaled from zero to one. Values are provided with a floating point data type. These transformations are especially useful for high spatial resolution DTMs, such as those derived from lidar [52].

Datasets and data augmentations

In order to use torch, data must be converted to tensors, or multidimensional arrays. The dataset class provided by torch can be subclassed to build pipelines to process data to tensors of required shapes and data types. An instance of the dataset subclass can then be used by a torch data loader to generate mini-batches of predictor variable chips and associated pixel-level labels during the training and validation processes. The geodl *defineSegDataSet()* function is implemented by subclassing the dataset class defined within torch. It accepts a data frame created by the *makeChipsDF()* function to read chip and mask files from disk and generate a single tensor of shape [Channels/Predictors, Width, Height] with a 32-bit float data type and an associated mask of shape [Class Indices, Width, Height] with a data type of long integer. It also provides a set of options for performing data rescaling (by dividing by a specified value), normalization to *z*-scores using band means and standard deviations, and random augmentations. Random augmentations are implemented with torchvision and include horizontal or vertical flips and augmentations of brightness, contrast, gamma, hue, and saturation. The user is able to specify the probability that an augmentation will be performed, the maximum number of augmentations to apply to a single chip, and the range of augmentation-specific parameters from which to select a random value. The goal

of performing these augmentations is to potentially combat overfitting [53,54]. Note that if a chip is flipped, the mask will also be flipped to maintain alignment.

Once an instance of *defineSegDataSet()* is instantiated, it can be provided to the *dataloader()* function from torch to define a data loader, which provides mini-batches of tensors during the training and validation processes. A mini-batch of predictor variables and associated masks provided by the data loader can be visualized using *viewBatch()* while *describeBatch()* provides a check of a data batch by returning the batch size; data type, dimensionality, and shape of the predictor variables and masks tensors; predictor variable means and standard deviations; and count of pixels mapped to each class index.

UNet-based models

Model overview

The UNet architecture was proposed by Ronnenberger et al. in 2015 for semantic segmentation of biomedical imagery [55]. Since its inception, it has expanded into a more general framework. UNet-like architectures share several common components; they consist of an encoder that is used to learn spatial relationships at multiple scales via learnable convolution kernels that are applied to input data or prior feature maps to generate new feature maps. The encoder is broken into separate blocks that consist of 2D convolution layers, activation functions (e.g., rectified linear unit (ReLU)), and, commonly, batch normalization. Each block is separated by a max pooling operation, which reduces the size of the array in the spatial dimensions and aids in allowing for learning patterns at varying spatial scales. The bottleneck separates the encoder and decoder components and represents the stage at which the data have been reduced to the smallest spatial resolution within the architecture. The purpose of the decoder is to restore the spatial resolution of the data in order to make pixel-level predictions as opposed to scene-level predictions. Similar to the encoder, the decoder is separated into blocks consisting of 2D convolution layers, activation functions, and batch normalization. Instead of decreasing the size of the array in the spatial dimensions using max pooling, the array is upsampled using either resampling algorithms, such as bilinear interpolation, or transpose convolution, which allows for upsampling with learnable kernels. Between encoder and decoder blocks with the same spatial resolution, skip connections are added that allow for semantic information to be shared across the model. Lastly, the pixel-level classification is performed using 1×1 2D convolution to return logits for each class that is differentiated [55].

The *defineUNet()* function provides a flexible means to generate a UNet-like architecture for semantic segmentation tasks. This architecture is conceptualized in Fig 4 and its associated parameters are described in Table 3. It can accept a variable number of input predictor variables and output classes and predicts a logit at each pixel location (i.e., the raw predictions are not rescaled to sum to one at each pixel location using a softmax function). It contains four encoder blocks, a bottleneck block, and four decoder blocks, and the user can specify the number of output feature maps from each block. The default number of output encoder feature maps per encoder block are 16, 32, 64, and 128; the default number of output feature maps for the bottleneck is 256; and the default number of output feature maps for the decoder blocks are 128, 64, 32, and 16. By default, rectified linear unit **(**ReLU**)** activation functions are implemented throughout the architecture to incorporate non-linearity, and batch normalization is used to combat gradient issues and aid in convergence. The user can replace the ReLU activations with either leaky ReLU or swish. In the encoder, the size of the array in the spatial dimensions is reduced by half following each block using 2×2 max pooling with a stride of two and a padding of zero. In the decoder, 2D transpose convolution is used to double the spatial resolution of the feature maps provided from

the prior block, also using a stride of two and a padding of zero. The final class logits are predicted from the final set of feature maps generated by the final decoder block using 1×1 2D convolution. A variety of optional configurations or modules can be added to the architecture including residual connections, squeeze and excitation modules, attention gates, an atrous spatial pyramid pooling (ASPP) module as the bottleneck block, and/or deep supervision. These additional modules are described in the following sections.

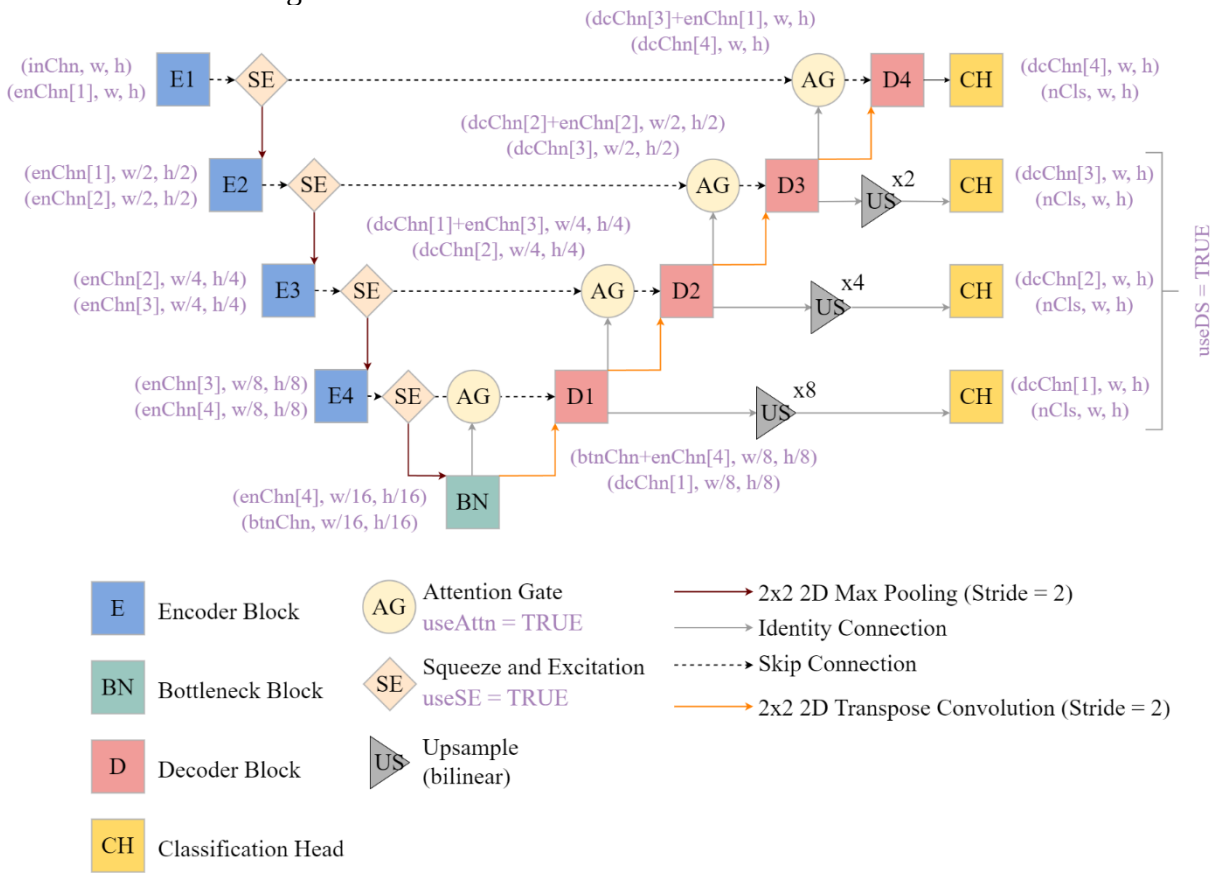

Fig 4. UNet architecture implemented in geodl and associated modules. w = width, h = height. Purple text corresponds to function parameters as implemented in geodl.

Table 3. *defineUNet()* function parameters.

Parameter	Explanation
inChn	Number of input channels or predictor variables
nCls	Number of classes being differentiated
actFunc	Activation function to use (ReLU, leaky ReLU, or swish)
useAttn	Whether or not to include attention gates along skip connections
useSE	Whether or not to include squeeze and excitation modules in the encoder blocks
useRes	Whether or not to include residual connections throughout the architecture
useASPP	Whether or not to replace the bottleneck block with an ASPP module
useDS	Whether or not to use deep supervision
enChn	Number of output feature maps produced by each encoder block
dcChn	Number of output feature maps produced by each decoder block
btnChn	Number of output feature maps produced by bottleneck block
dilRates	Dilation rates to use in ASPP module
dilChn	Number of feature maps produced by each branch in the ASPP module
negative_slope	Negative slope term to apply if leaky ReLU is used
seRatio	Squeeze and excitation reduction ratio

Activation functions

The ReLU activation function is used by default within the architecture. This function simply converts all negative activations to zero and maintains all positive activations as their original value (Equation 1) [8,56]. To combat the "dying ReLU" problem, it may be desirable to maintain negative activations, but with a reduced magnitude. Leaky ReLU accomplishes this by maintaining positive activations and multiplying negative activations by a positive value smaller than one (called a negative slope term in Equation 2) in order to reduce their magnitude (Equation 2) [57]. Another option is the swish activation, which is calculated by multiplying the activation by the activation modified using a sigmoid function (Equation 3) [58]. The *actFunc* parameter allows the user to use leaky ReLU or swish in place of ReLU. Note that none of these activation functions add trainable parameters to the model.

$$ReLU = \begin{cases} if\ activation < 0, 0 \\ else,\ activation \end{cases} \quad \text{(Equation 1)}$$

$$Leaky\ ReLU = \begin{cases} if\ activation < 0,\ x * negative\ slope\ term \\ else,\ activation \end{cases} \quad \text{(Equation 2)}$$

$$Swish = activation \cdot \text{sigmoid}(activation) \quad \text{Equation (3)}$$

Residual connections

The traditional double-convolution layers used in UNet consist of passing the input predictor variables or feature maps produced from prior layers through a 3×3 2D convolution block to produce a set of feature maps equal to the number of input feature maps. These results are then passed through a second 3×3 2D convolution layer to generate the user-defined number of output feature maps for that stage in the architecture [55]. This is conceptualized in Fig 5(a). Both convolution blocks use a stride and padding of one so that the input number of rows and columns of pixels are maintained.

A residual connection or residual block augments this architecture by adding the input feature maps directly to the output from the second 2D convolution (Fig 5(b)). Note that this is an actual addition of the feature maps, not a concatenation. The goal is to potentially reduce the

vanishing gradient issue by maintaining this original signal provided to the block in the output of the block [59]. Note that the input data are augmented along the residual path so that the number of input feature maps matches the number of feature maps generated by the convolution operations, since this is required to add the input and output tensors.

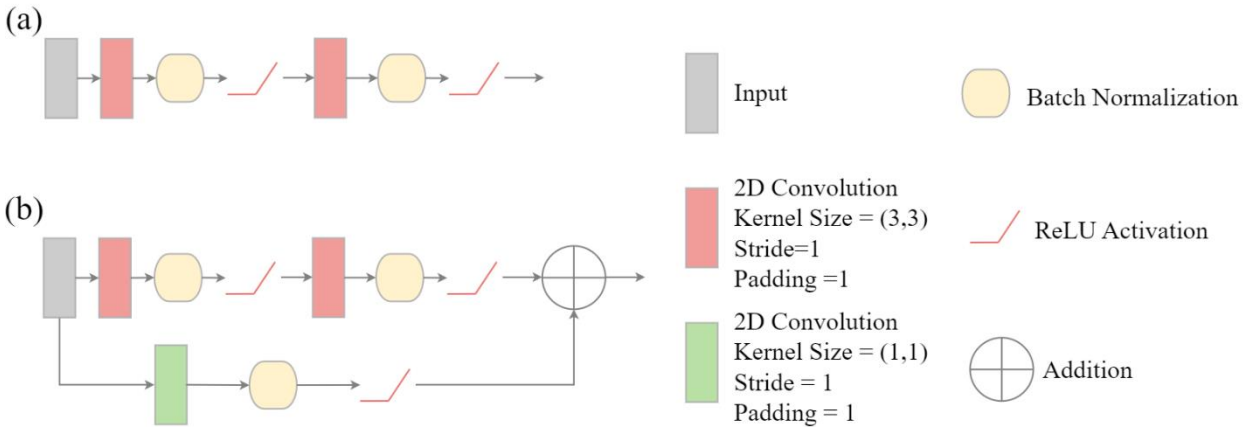

Fig 5. (a) double convolution block. (b) double convolution block with residual connection.

Squeeze and excitation module

The goal of a squeeze and excitation (SE) module is to capture interrelationships between channels or feature maps. Note that this is not the primary goal of traditional convolution operations, which instead focus on learning spatial relationships [60]. Fig 6 provides a conceptualization of this module. Fig 6(a) shows a version of the module that does not include a residual connection while Fig 6(b) does include a residual connection. The input data consist of channels or feature maps generated from prior convolution layers. First, each channel is reduced to a single value using global average pooling, resulting in a vector of input channel or feature map means. This is the "squeeze" component of the module where the information is reduced to a channel-wise summary metric. Following the global average pooling, the remainder of the module is the "excitation" component where the rescaling of the input data is guided by the learned interrelationships between the channels. First, the means are modified using a fully connected layer, ReLU activation, and a final fully connected layer. The goal of this sequence of operations is to model non-linear interrelationships between the means. The first fully connected layer has a smaller number of outputs than inputs, which is controlled by a user-defined reduction term (see Table 3). The final fully connected layer has an output size equal to the original number of channels or feature maps provided to the SE module. The output from the last fully connected layer is then passed through a sigmoid activation function to rescale the values to a range of zero to one. The input channels or feature maps are then multiplied by the rescaled values on a per channel basis to augment the input data.

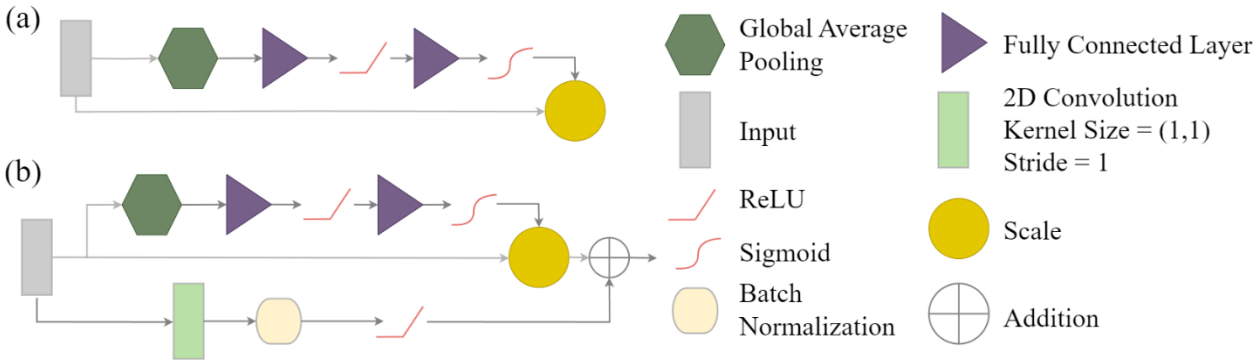

Fig 6. Squeeze and excitation (SE) module after Hu et al. (2018) optionally implemented in the encoder component of geodl's UNet architecture.

Attention gates

An attention gate (AG) module provides a mechanism to allow for forcing the model to focus on key features or regions within the image [61,62]. The idea is to use the results from the subsequent layer in the network, where a deeper set of features have been extracted, to add focus, or attention, to the feature maps from the prior layer that are then concatenated with the upscaled feature maps from the following block and fed to the decoder block. This process is conceptualized in Fig 7. The feature maps from the next layer in the sequence (for example, the feature maps produced by decoder block three when the attention gate is applied to the feature maps from encoder block two) are passed through a 1×1 2D convolution layer with a stride of one and a padding of zero. The number of channels is changed to match those from the prior block. A batch normalization is then applied. The feature maps from the current layer are passed through a 1×1 2D convolution layer with a stride of two and a padding of zero. The number of output feature maps is equal to the number of input feature maps. Since a stride of two is used, the spatial resolution is reduced by half such that the size is the same as those from the next block. Batch normalization is then applied. The gating signal and augmented feature maps are then added together and passed through a ReLU activation. This result is then passed through a 1×1 2D convolution with a stride of one and a padding of zero to produce a single output feature map. This feature map is then passed through a batch normalization layer followed by a sigmoid activation. This results in values between zero and one where values near one highlight areas that should be focused on or areas to which attention should be applied. In order to return the original spatial resolution of the input feature maps, upsampling is then applied using bilinear interpolation. The original feature maps from the encoder block of interest are multiplied by this upscaled result. Lastly, the results are concatenated with the upsampled feature maps from the next block, which are first upscaled using 2D transpose convolution, to be fed into the associated decoder block as normal [61,62].

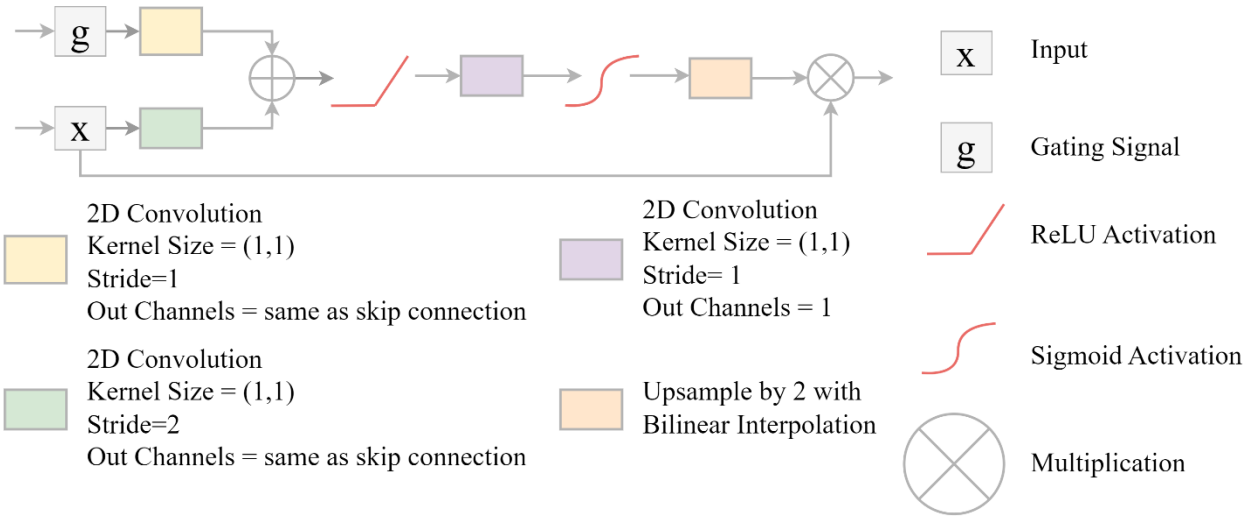

Fig 7. Attention gate (AG) module after Abraham and Khan (2018) and Oktay et al. (2018) optionally implemented along skip connections of geodl's UNet architecture.

Atrous spatial pyramid pooling (ASPP) module

Atrous spatial pyramid pooling (ASPP) is similar to the concept of dilated convolution. The goal is to capture spatial context information at varying scales by increasing the size of the receptive field. This technique is applied within the DeepLabv3+ architecture [63–65]. We implement a modified version of this module here (Fig 8) as an optional replacement for the traditional UNet bottleneck layer. Fig 8(a) conceptualizes the module without a residual connection while Fig 8(b) includes a residual connection. This module accepts the feature maps from the fourth encoder block following max pooling. Dilated convolution is then performed using dilation rates of 1, 2, 4, 8, and 16 by default. These rates can be specified by the user. By default, 16 feature maps are generated by each of the dilated convolution layers; however, this can also be changed by the user. The total number of feature maps produced is five times the number of feature maps generated by each dilated convolution layer since there are five branches within the ASPP module. The results are then concatenated and passed through a 1×1 2D convolution layer with a stride of one and a padding of zero to reduce the number of total feature maps returned.

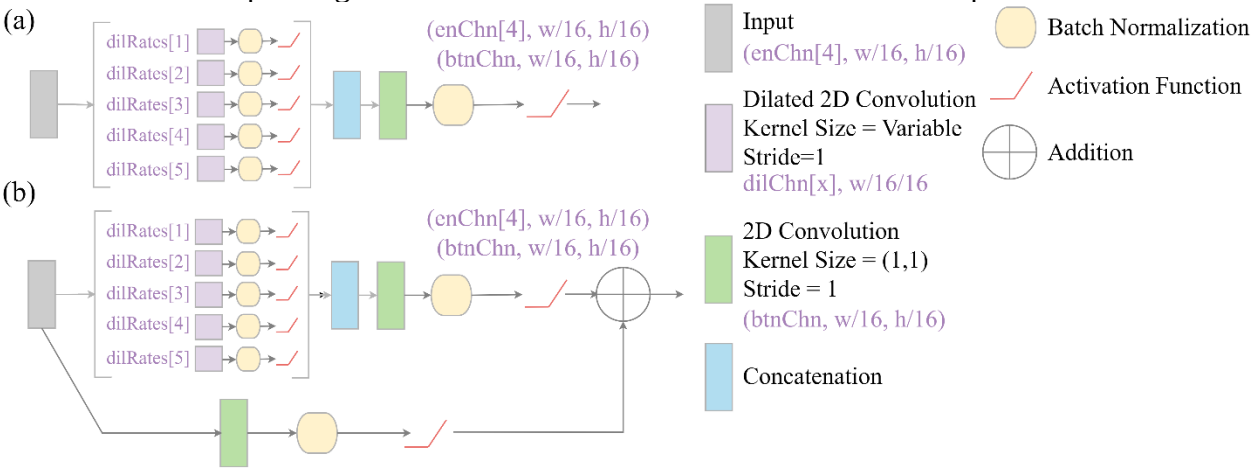

Fig 8. Modified atrous spatial pyramid pooling (ASPP) module inspired by the DeepLabv3+ architecture and optionally implemented as a replacement bottleneck layer of geodl's UNet architecture. w = width, h = height.

Deep supervision

In the context of a UNet-like architecture, the goal of deep supervision is to offer additional training guidance within the intermediate layers of the architecture by calculating auxiliary losses generated using the feature maps from that stage in the architecture [66–69]. The feature maps produced by decoder blocks one, two, and three are upsampled to match the original resolution of the input data using bilinear interpolation. Next, 1×1 2D convolution is used to predict logits for each class at each pixel location using the feature maps generated by each decoder block separately. See Fig 4 above. These ancillary predictions are then compared to the associated mask to calculate additional losses that can then be combined with the results from the final decoder block. Further, the user can control the relative weight of each of the four losses in the final loss calculation. This will be discussed in more detail below in the context of our unified focal loss implementation.

UNet with MobileNet-v2 encoder

A second UNet model has also been included as part of this package. The *defineMobileUNet()* function defines a UNet architecture with a MobileNet-v2 backbone or encoder (Fig 9) [48,70]. The MobileNet-v2 architecture is a lightweight CNN for use on mobile devices that incorporates many design innovations including depth-wise separable convolution and inverted residual and linear bottleneck layers [48]. This UNet implementation was inspired by a blog post by Sigrid Keydana [71,72]. It has six blocks in the encoder (including the bottleneck) and five blocks in the decoder. The user is able to implement deep supervision and/or attention gates as described above. Residual connections and squeeze and excitation modules are not implemented. The model can be initialized using pre-trained weights based on ImageNet [73], and the encoder can be frozen (i.e., made not trainable during the learning process). Since this architecture makes use of ImageNet-based weights, it can currently only accept predictor variables with three input channels.

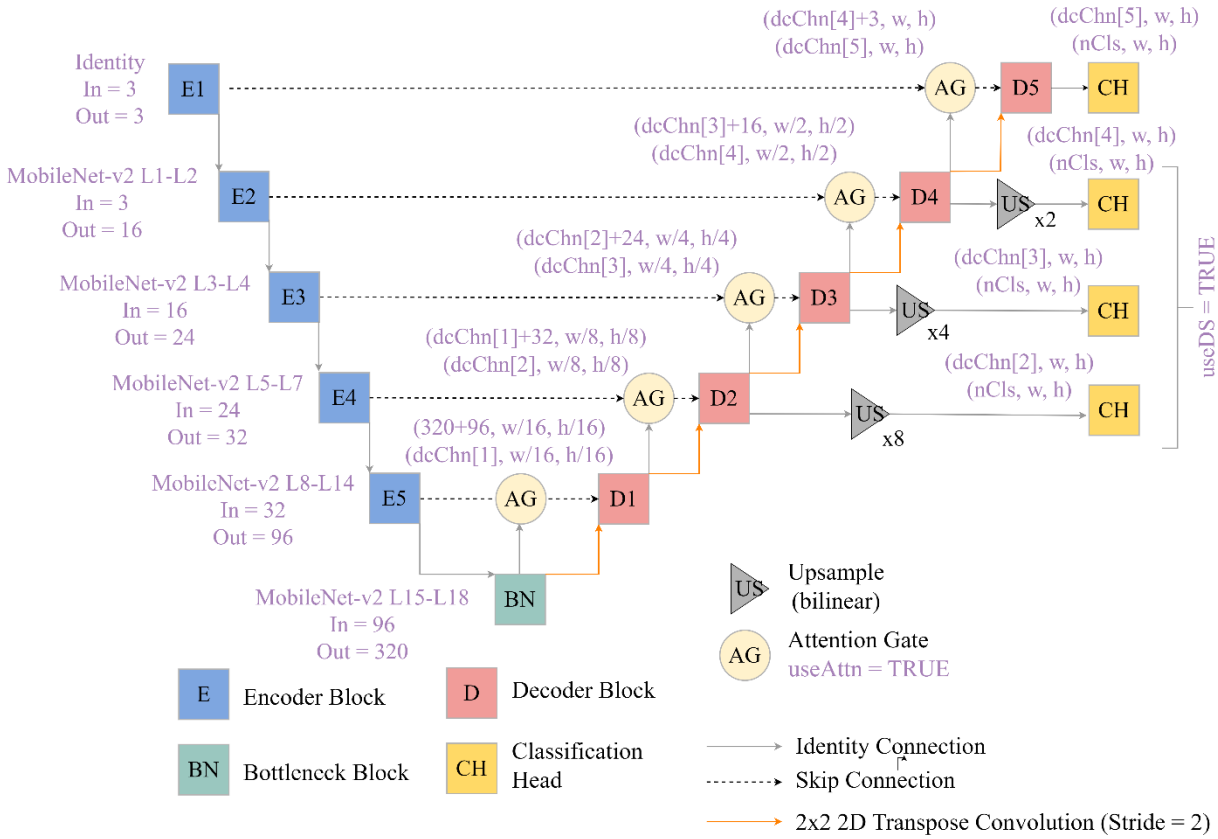

Fig 9. UNet with MobileNet-v2 encoder, attention gates along skip connections, and deep supervision as implemented in geodl. L = layer, w = width, h = height.

Training, validation, and inference

Loss metrics

Since this package treats all classification problems as multiclass, multiclass loss metrics must be used. Specifically, cross entropy (CE) loss should be used as opposed to binary cross entropy (BCE) loss. Again, this is because both the background and positive case logits are returned when only two classes are differentiated, as opposed to only returning the positive case prediction, as is required to use BCE loss. The choice of loss metric is very important, as this measure serves as the sole guide to updating the model parameters during the learning process using backpropagation of errors and the optimization algorithm.

Additional loss metrics have been proposed that can be especially useful when class proportions in the training set are imbalanced, which is a common occurrence in spatial predictive modeling, and/or when the user desires more control over the relative weightings of false positive (FP) and false negative (FN) errors relative to specific classes. The Dice (Equation 4) [74,75] or Tversky (Equation 5) [76] loss is often used, which are generally termed region-based losses. Since the Dice score is actually and accuracy measure, Dice loss is calculated as 1 − Dice, and since Dice and F1-score are equivalent [77], it can also be calculated as 1 − F1-score. The Tversky loss allows for specifying the relative weights of FN and FP errors using alpha and beta terms, respectively. Dice- and Tversky-based losses make use of the rescaled class logits, obtained by applying a sigmoid or softmax activation, as opposed to the "hard" classification, as is the case when Dice, or the equivalent F1-score, is used as an accuracy assessment metric of the final output. Other options

include macro-averaging, which gives equal weight in the aggregated assessment metric, or weighted macro-averaging, which allows the user to control the relative weight of the classes [74–76,78,79]. We do not implement micro-averaging, because that method is equivalent to overall accuracy, and thus is sensitive to class proportions in the training data set [78].

Focal losses, such as focal CE, focal Dice, and focal Tversky, allow for adding additional weight to difficult-to-predict samples or classes, which are defined as those that have a low predicted rescaled logit for their correct class. For focal CE loss, this weighting is applied sample-by-sample. In contrast, for Dice or Tversky, the weighting is applied class-by-class [61,79,80].

$$\text{Multiclass macro-averaged Dice loss} = \frac{1}{N}\sum_{j=1}^{C}\left(1 - \left(\frac{(2 \times \Sigma\hat{p}_{TP}) + \varepsilon}{(2 \times \Sigma\hat{p}_{TP}) + \Sigma\hat{p}_{FN} + \Sigma\hat{p}_{FP} + \varepsilon}\right)\right) \quad \text{(Equation 4)}$$

$$\text{Multiclass Tversky loss} = \frac{1}{N}\sum_{\text{j}}\left(1 - \left(\frac{\Sigma\hat{p}_{TP}) + \varepsilon}{\Sigma\hat{p}_{TP} + \alpha\Sigma\hat{p}_{FN} + \beta\Sigma\hat{p}_{FP} + \varepsilon}\right)\right) \quad \text{(Equation 5)}$$

The torch package provides implementations of the BCE and CE losses. However, it does not provide implementations of the Dice or Tversky losses or focal versions of any losses. In order to expand the range of loss functions available, we implemented a modified version of the unified focal loss proposed by Yeung et al. [81]: *defineUnifiedFocalLoss()*. When implementing deep supervision, the *defineUnifiedFocalLossDS()* version should be used, which allows for specifying the relative weights of each of the four losses. This loss is configured for multiclass problems to align with the design of the package. If it will be used for a classification where only two classes are differentiated, the model must return logits for both the positive and negative/background classes. Our implementation of the unified focal loss is modified from the implementation originally proposed by Yeung et al. Modifications from the original implementation include: (1) allowing users to define separate class weights for both the distribution-based and region-based metrics, (2) using class weights as opposed to the symmetric and asymmetric methods implemented by the authors, and (3) including an option to apply a logcosh transform for the region-based loss, which can help stabilize the learning process by providing smoother gradients [82]. Equation 6 describes the implemented modified unified focal loss while the modified focal CE loss component is provided in Equation 7 and the modified Tversky loss is provided in Equation 8. The equation for the modified Tversky index, on which the modified Tversky loss is based, is provided in Equation 9.

$$\text{Modified unified focal loss} = \lambda \times \text{mFL} + (1 - \lambda) \times \text{mTL} \quad \text{(Equation 6)}$$

$$\text{Modified focal CE loss (mFL)} = -\frac{1}{\sum_{i=1}^{n} w_j}\sum_{i=1}^{n}\sum_{j=1}^{C} w_j\left[\left(1 - \widehat{y_{ij}}\right)^{1-\gamma} \cdot y_{ij} \cdot \log\left(\widehat{y_{ij}}\right)\right] \quad \text{(Equation 7)}$$

$$\text{Modified Tversky loss (mTL)} = \frac{1}{\sum_{j=1}^{C} w_j}\sum_{j=1}^{C} w_j(1 - mTI_{\text{j}})^{\gamma} \quad \text{(Equation 8)}$$

$$\text{Modified Tversky Index (mTI)} = \left(\frac{\Sigma\hat{p}_{TP}) + \varepsilon}{\Sigma\hat{p}_{TP} + \delta\Sigma\hat{p}_{FN} + (1-\delta)\Sigma\hat{p}_{FP} + \varepsilon}\right) \quad \text{(Equation 9)}$$

As described in Table 4, by adjusting the lambda (λ), gamma (γ), delta (δ), and class weight terms (*clsWghtsDist* and *clsWghtsReg*), the user can implement a variety of different loss metrics including CE loss, weighted CE loss, focal CE loss, focal weighted CE loss, Dice loss, focal Dice loss, Tversky loss, and focal Tversky loss. λ controls the relative weight of the distribution- and region-based losses. The default is 0.5, or equal weighting between the losses is applied. If λ = 1, only the distribution-based loss is considered. If λ = 0, only the region-based loss is considered. Values between 0.5 and 1 put more weight on the distribution-based loss while values between 0 and 0.5 put more weight on the region-based loss. γ controls the application of focal loss and the application of increased weight to difficult-to-predict pixels (for the distribution-based loss) or difficult-to-predict classes (for the region-based loss). Smaller γ values put increased weight on difficult samples or classes. Using a γ of 1 equates to not using a focal adjustment. The δ term

controls the relative weight of FP and FN errors for each class. The default is 0.6 for each class, which results in placing a higher weight on FN as opposed to FP errors relative to each class [81].

Table 4. Modified unified focal loss framework parameterization after Yeung et al. (2022).

	Distribution-Based	**Compound**	**Region-Based**
	$\lambda = 1$	$\lambda < 1$ & $\lambda > 0$	$\lambda = 0$
$\gamma > 0$ & $\gamma < 1$ $\delta \neq 0.5$	Focal CE Loss	Unified Focal Loss	Focal Tversky Loss
$\gamma = 1$ $\delta \neq 0.5$	CE Loss	Tversky + CE Loss	Tversky Loss
$\gamma = 1$ $\delta = 0.5$	CE Loss	CE + Dice Loss	Dice Loss

clsWghtsDist = relative weighting of classes in distribution-based loss (applied to each sample)
clsWghtsReg = relative weighting of classes in region-based loss (applied to each class when calculating a macro average)
useLogCosH = whether or not to apply a log cosh transformation to the region-based loss

The deep supervision version of the loss (*defineUnifiedFocalLossDS()*) expects four predictions, and the user can specify the relative weightings of each loss in the final loss, which is simply calculated as the weighted average of the four losses. The default weights are 0.6, 0.2, 0.1, and 0.1. The first weight is applied to the result from the final decoder block while the subsequent weights are applied to the results from the third, second, and first decoder blocks, respectively (see Fig 4). If the MobileNet-v2 UNet version is used, the fifth through second decoder blocks are used (see Fig 9).

Assessment metrics

Several assessment metrics are provided by the luz package. For example, *luz_metric_accuracy()* calculates overall accuracy for a multiclass classification. luz also provides the *luz_metric()* function to allow users to define new or custom metrics [46]. The geodl package makes use of this function to create implementations of recall, precision, and F1-score. It also includes a version of the overall accuracy (OA) metric (*luz_metric_overall_accuracy()*) that accepts predictions and targets defined with the shapes and data types used within the package for standardization. Table 5 provides descriptions of the implemented assessment metrics. Macro-averaging is used in which the metric is calculated separately for each class and then averaged. Each class has equal weight in the resulting metric by default; however, user's can choose to apply relative weightings. This is especially useful for binary classification problems when the user wishes to calculate precision, recall, and F1-score for only the positive case as opposed to averaging these metrics for both the positive and negative cases. To obtain this result, the user must assign the background class a weight of zero and the positive case a weight of one. It is important to note that recall, precision, F1-score, and overall accuracy are all equivalent when micro-averaging is used [78,83,84]; therefore, micro-averaging is not implemented here. As noted in Table 5 and in alignment with terminology used in remote sensing, class-level recalls are equivalent to producer's accuracies (1 – omission error) while class-level precisions are equivalent to user's accuracies (1 – commission error) [85,86]. As a result, our metrics return macro-averaged, class aggregated producer's and user's accuracies.

Table 5. Accuracy assessment metrics implemented in geodl.

Metric	Function	Equation	Notes
Overall Accuracy (OA)	*luz_metric_overall_accuracy()*	$\frac{\text{Total Correct}}{\text{Total Samples}}$	
Precision	*luz_metric_precision()*	$\frac{1}{N}\sum_{j=1}^{C}\frac{\text{TP}_j}{\text{TP}_j + \text{FP}_j}$	Equivalent to average of class-level producer's accuracies
Recall	*luz_metric_recall()*	$\frac{1}{N}\sum_{j=1}^{C}\frac{\text{TP}_j}{\text{TP}_j + \text{FN}_j}$	Equivalent to class-level user's accuracies
F1-Score	*luz_metric_f1score()*	$\frac{2 \times \text{Recall} \times \text{Precision}}{\text{Recall} + \text{Precision}}$	Harmonic mean of precision and recall

Other training and validation considerations

We recommend using the luz package both to train and assess models, as implementing custom training and validation loops is error prone. The torch and luz documentation provides examples of training processes: https://torch.mlverse.org/. Also, the code provided as supporting material for this paper to accompany the associated case studies can be modified for new tasks. The torch package provides access to many common optimization algorithms including mini-batch stochastic gradient descent [8,87–89], Adagrad [90], Adadelta [91], RMSprop [92], Adam [93], and AdamW [94]. We generally use AdamW as our default optimization algorithm; however, users may consider exploring alternatives.

Generally, the learning rate is an important hyperparameter. A large learning rate may cause the optimization process to pass over the optimal parameters. In contrast, a low learning rate may cause the learning process to get "stuck" in a local minimum and/or require excessive time for the learning process to converge [8]. One means to select a learning rate is described by Smith [95,96]. This learning rate finder process works by running a fast training iteration where the learning rate starts at a very low value and is incrementally increased to a very large value with the learning rate changing after each data mini-batch is processed. The optimal learning rate is not the one associated with the minimum loss; instead, it is the one with the associated largest negative slope or gradient. The best range of losses is generally associated with this region of rapidly decreasing loss. The luz package provides an implementation of a learning rate finder via the *lr_finder()* function [46]. Generally, we suggest using this function to select an appropriate learning rate or range of learning rates.

luz also provides the *luz_callback_lr_scheduler()* function for defining and implementing callbacks to change or adapt the learning rate during the training process. This function can use a variety of learning rate schedulers provided by torch. We have found one-cycle learning to be useful and recommend that it be experimented with. The luz package provides additional callbacks that can be very useful during the learning process. For example, *luz_callback_early_stopping()* can be used to stop the learning process early if the model is no longer improving based on the loss or an assessment metric of interest, either calculated from the training or validation data. *luz_callback_csv_logger()* allows for logging calculated losses and metrics for the training and validation data to disk as a CSV file. *luz_callback_model_checkpoint()* can be used to save models

to disk after each epoch or only if the model has improved based on the loss or an assessment metric. Custom callbacks can be defined using the *luz_callback()* function [46].

Model assessment and spatial predictions

Once a model has been trained, the results should be assessed using a testing dataset that is separate and non-overlapping with the training and validation sets [85,86,97–100]. geodl provides several functions for assessing models. The *viewBatchPreds()* function allows for visualizing a batch of predictions, reference masks, and predictor variables that were created using *defineSegDataSet()* and a data loader, and subsequently predicted with a trained model. The luz package provides additional routines, which are demonstrated in our examples, for obtaining accuracy assessment metrics and losses for an entire testing set fed to the model as mini-batches. Effectively, this process implements the same loss and accuracy assessment calculations used in the training loop for the training and validation data. geodl provides an *assessDL()* function for calculating assessment metrics from a data loader. It also provides the *assessPnts()* function that allows for performing assessments at point locations. This requires that reference and predicted classes be extracted at point locations and stored in a data frame. The *assessRaster()* function allows for assessment using all cells in an extent as opposed to point locations. This method can be used when reference labels and predictions are available for all pixels in an extent.

These functions generate a set of summary metrics when provided reference and predicted classes. A confusion matrix is produced with the columns representing the reference data and the rows representing the predictions. The following metrics are calculated: overall accuracy (OA), average class user's accuracy (i.e., precision), average class producer's accuracy (i.e., recall), and average class F1-score. For average class user's accuracy, producer's accuracy, and F1-score, macro-averaging is used where all classes are equally weighted. As mentioned above, it is not necessary to return micro-averaged producer's accuracy, user's accuracy, and F1-score since they are equivalent to overall accuracy [78,83,84]. We do not include the Kappa statistic since its use in remote sensing is now being discouraged [101,102]. All class user's and producer's accuracies are also returned. For assessing map output, we generally recommend using a testing set that honors the true landscape proportions of each class. When a confusion matrix is generated using proportions that approximate the true landscape proportions, it is termed an estimated population matrix or estimated population confusion matrix [103].

A trained model can be used to infer to new raster data as long as the input variables are the same as those used to train the model. The *predictSpatial()* function allows for predicting to a raster extent. In order to process large raster extents, chips are extracted from the larger extent relative to the *chpSize* parameter. Overlap between chips are specified using the *stride_x* and *stride_y* parameters. We generally recommend using an overlap of at least 25% between adjacent chips. It has generally been found that predictions nearer to the margin of a chip have lower accuracy than those in the interior of the chip, likely due to the lack of a full set of neighboring pixels. As a result, the *crop* parameter can be set to remove outer rows and columns of pixels and not include them in the final, merged product. Using an overlap via the *stride_x* and *stride_y* parameters in combination with cropping (*crop*) allows for only predictions in the center of each processed chip to be included in the final, merged product. The *predType* parameter controls the type of prediction returned. If it is set to "class", the "hard" classification is returned. If the *predType* parameter is set to "logit", the raw logit for each predicted class is returned, without any rescaling, and a multiband raster grid is generated where each band provides the logit for a specific class. If *predType* is set to "probs", the raw logits are rescaled by passing them through a softmax activation. This results in all class predictions at a pixel location summing to one. It is also

important that data being predicted be rescaled and/or normalized using the same settings defined for the training dataset.

Case studies

In this section, we present some sample classification results obtained using geodl. Code for these experiments have been provided in the associated FigShare repository; the classificationExampleTopoDL.R file provides the workflow for the classification of the topoDL dataset while the classificationExampleLCAI.R file provides the workflow for the landcover.ai dataset. These examples can be modified to build workflows for new datasets.

Surface mine disturbance from historic topographic maps

Within our topoDL example, 3,886 256-by-256 cell image chips were used to train the model while 812 chips were used to validate the model at the end of each training epoch, and 1,246 were maintained as a testing set to assess the final model. The data were partitioned such that all chips from the same topographic map were included in the same data partition in order to avoid spatial autocorrelation between the data partitions. For the training set, a maximum of one augmentation was performed per chip, either a vertical or horizontal flip with a 0.5 probability of being applied. A mini-batch size of 15 was used and the model was trained for ten epochs. The model that returned the lowest loss for the validation data was maintained as the final model. The modified unified focal loss was configured as a Tversky loss using $\lambda = 0$, $\gamma = 1$, and $\delta = 0.6$. In other words, only the region-based loss was included with no focal adjustment but unequal weighting for FN and FP errors per class. The AdamW optimizer was used with a learning rate of 1e-3, which was selected using the learning rate finder implementation in the luz package. Training was conducted using the luz package.

Table 6 provides the confusion matrix and derived metrics calculated from it for the withheld testing set and using the *assessDL()* function while Fig 10 provides an example set of image chips (a), reference masks (b), and predictions (c) for a batch of testing samples created using the *viewBatchPreds()* function. Note that the values are large since the table represents all cells from all chips in the testing set. The overall accuracy for the prediction was 0.987 while the F1-score for the mine class was 0.954. The precision was 0.945 while the recall was 0.963, suggesting a good compromise between commission and omission errors.

Table 6. Confusion matrix and derived metrics for topoDL [43] classification. Values represent counts of pixels or cells. NPV = negative predictive value.

		Reference		
		Background	Mine	
Prediction	Background	69,669,489	416,686	NPV = 0.994
	Mine	635,137	10,871,008	Precision = 0.945
		Specificity = 0.991	Recall = 0.963	F1-Score = 0.954 OA = 0.987

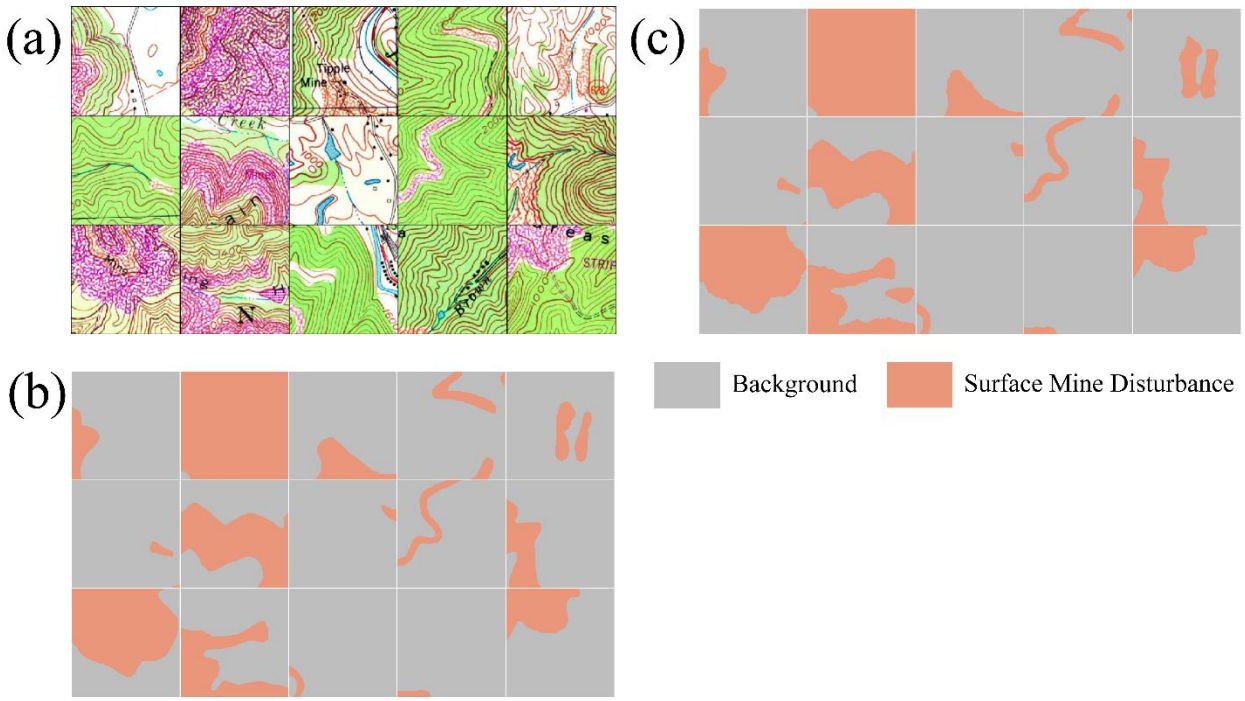

Fig 10. Example prediction of surface mine disturbance extents from topoDL dataset [43].

Landcover.ai multiclass land cover classification

For the landcover.ai experiment, 3,000 512-by-512 cell image chips were used to train the model while 500 were used to validate the model at the end of each training epoch, and 500 were maintained as a testing set to assess the final model. Data partitions were defined by the data originators. For the training set, a maximum of one augmentation was performed per chip, either a vertical flip, horizontal flip, brightness adjustment, or saturation adjustment with probabilities of being applied of 0.5, 0.5, 0.1, and 0.2, respectively. A mini-batch size of 15 was used, and the model was trained for ten epochs. The model that returned the lowest loss for the validation data was maintained as the final model. The modified unified focal loss was configured as a focal Dice loss using $\lambda = 0$, $\gamma = 0.8$, and $\delta = 0.5$. In other words, only the region-based loss was included, a focal adjustment was applied to increase the relative cost of misclassifying difficult classes, and FN and FP errors per class were equally weighted. The AdamW optimizer was used with a learning rate of 1e-3, which was selected using the learning rate finder implementation in the luz package. Training was conducted using the luz package.

Table 7 provides the confusion matrix and class-level user's and producer's accuracies calculated for the withheld testing set and using the *assessDL()* function while Table 8 provides the overall accuracy (OA) and macro-averaged, class-aggregated F1-score (aF1), producer's accuracy (recall) (aPA), and user's accuracy (precision) (aUA). Fig 11 provides an example set of image chips (a), reference masks (b), and predictions (c) for a batch of testing samples created using the *viewBatchPreds()* function. An overall accuracy of 0.932 and a macro-averaged F1-score of 0.839 were obtained. The woodland class had both the lowest producer's and user's accuracy. The building class also proved challenging to map.

Table 7. Confusion matrix and class-level user's and producer's accuracies for landcover.ai [44] classification.

		Reference					
		Background	Building	Woodland	Water	Road	User's Accuracy
Prediction	Background	55,986,258	254,781	442,870	252,298	1,911,020	0.951
	Building	91,224	540,680	559	1,966	485	0.852
	Woodland	339,710	31,473	1,050,509	1,549	12,865	0.732
	Water	538,653	155	226	3,978,067	88,367	0.864
	Road	2,893,064	10,879	179,322	56,208	35,145,836	0.918
	Producer's Accuracy	0.936	0.645	0.628	0.927	0.946	

Table 8. Overall accuracy and macro-averaged class aggregated assessment metrics for landcover.ai [44] classification. OA = overall accuracy, aF1 = macro-averaged, class aggregated F1-score, aPA = macro-averaged, class aggregated producer's accuracy (recall), aUA = macro-averaged, class aggregated user's accuracy (precision).

OA	**aF1**	**aPA**	**aUA**
0.932	0.839	0.816	0.863

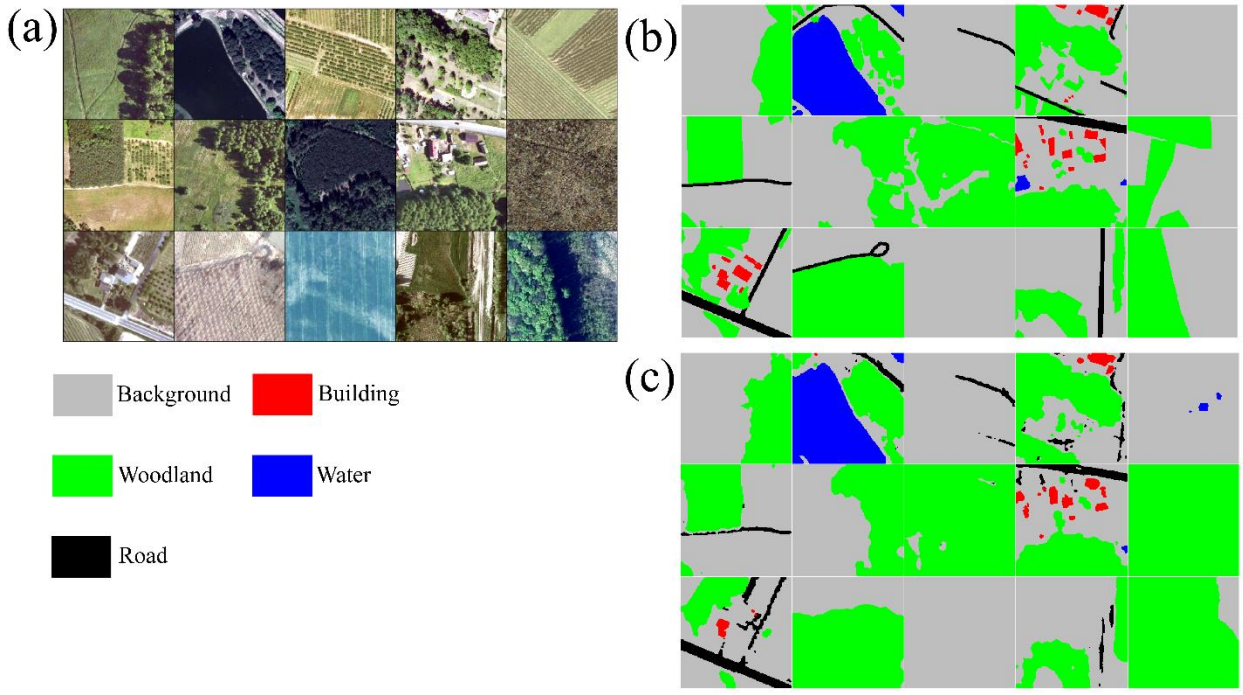

Fig 11. Example prediction of general land cover from landcover.ai dataset [44].

Conclusions and future development

The goal of geodl is to provide a complete workflow as an R-based tool to perform DL-based semantic segmentation that adheres to standards and best practices within geospatial predictive modeling and remote sensing. The use of the torch package simplifies the software stack since it is not necessary to interface with a Python environment and associated libraries. It also supports the use of GPU-based computation, which is necessary for practical use of DL applied to large datasets. The use of terra allows for efficient handling of large raster datasets with varying number of bands. Lastly, luz greatly simplifies the DL training and validation processes and the placement and transfer of models and data between the CPU and GPU. We argue that geodl provides an intuitive workflow applicable to a wide variety of geospatial semantic segmentation problems and input data that can be represented as multidimensional arrays. It makes well established DL workflows and UNet-like architectures available to geospatial, remote sensing, and Earth scientists, and is particularly useful for users who are more comfortable in the R environment than other languages, such as Python. In such cases, geodl can also be useful for extracting features from models trained with specific geospatial data followed by using these features to perform targeted prompting of Foundation Models [104] for image segmentation such as the Segment Anything Model (SAM) [105], which can then generate more relevant or informative outputs.

We plan to further develop geodl with future releases. First, we plan to implement a torch dataset subclass that allows for sampling from larger raster grids dynamically as opposed to generating image chips, similar to the implementation in the geotorch Python package [106]. We plan to implement additional CNN-based models including UNet3+ [69] and DeepLabv3+ [63,64,107]. Generally, we would like to provide a wider range of semantic segmentation algorithms and backbones, similar to the segmentation models Python package [108]. Additional development of loss functions would also be valuable, such as the ability to weight pixels based on their distance from class boundaries. We would also like to expand the package to include transformer-based segmentation DL architectures, such as SegFormer [109]. We would also like to provide additional functions for customizing the training loop, such as using different learning rates for different components of the model architecture. We are interested in finding others to contribute to the package. Ultimately, we hope that geodl is a useful contribution to the torch ecosystem in R.

Data Availability

The data and example code are available on FigShare: https://figshare.com/articles/dataset/geodl_example_data/23835165. The geodl package source code is available on GitHub: https://github.com/maxwell-geospatial/geodl. It can be downloaded and installed using the remotes package. At the time of this writing, we are working toward submitting the package to the Comprehensive R Archive Network (CRAN) for consideration for inclusion in the archive.

References

1. Hoeser T, Bachofer F, Kuenzer C. Object Detection and Image Segmentation with Deep Learning on Earth Observation Data: A Review—Part II: Applications. Remote Sens. 2020;12: 3053. doi:10.3390/rs12183053
2. Hoeser T, Kuenzer C. Object Detection and Image Segmentation with Deep Learning on Earth Observation Data: A Review-Part I: Evolution and Recent Trends. Remote Sens. 2020;12: 1667. doi:10.3390/rs12101667
3. Yuan Q, Shen H, Li T, Li Z, Li S, Jiang Y, et al. Deep learning in environmental remote sensing: Achievements and challenges. Remote Sens Environ. 2020;241: 111716. doi:10.1016/j.rse.2020.111716
4. Maxwell AE, Warner TA, Fang F. Implementation of machine-learning classification in remote sensing: An applied review. Int J Remote Sens. 2018;39: 2784–2817.
5. Zhang L, Zhang L, Du B. Deep learning for remote sensing data: A technical tutorial on the state of the art. IEEE Geosci Remote Sens Mag. 2016;4: 22–40.
6. Zhu XX, Tuia D, Mou L, Xia G-S, Zhang L, Xu F, et al. Deep learning in remote sensing: A comprehensive review and list of resources. IEEE Geosci Remote Sens Mag. 2017;5: 8–36.
7. Long J, Shelhamer E, Darrell T. Fully convolutional networks for semantic segmentation. Proceedings of the IEEE conference on computer vision and pattern recognition. 2015. pp. 3431–3440.
8. Zhang A, Lipton ZC, Li M, Smola AJ. Dive into Deep Learning. Cambridge University Press; 2023.
9. Desktop GIS Software | Mapping Analytics | ArcGIS Pro. [cited 23 Apr 2024]. Available: https://www.esri.com/en-us/arcgis/products/arcgis-pro/overview
10. Image Analysis Software | ArcGIS Image Analyst for ArcGIS Pro. [cited 23 Apr 2024]. Available: https://www.esri.com/en-us/arcgis/products/arcgis-image/options/arcgis-image-analyst
11. Image Processing & Analysis Software | Geospatial Analysis Software | ENVI®. [cited 23 Apr 2024]. Available: https://www.nv5geospatialsoftware.com/Products/ENVI
12. ENVI® Deep Learning Software | Geospatial Deep Learning Technology. [cited 23 Apr 2024]. Available: https://www.nv5geospatialsoftware.com/Products/ENVI-Deep-Learning
13. Igual L, Seguí S. Introduction to Data Science. Introduction to Data Science. Springer; 2017. pp. 1–4.
14. Wickham H, Grolemund G. R for data science: import, tidy, transform, visualize, and model data. O'Reilly Media, Inc.; 2016.
15. Welcome to Python.org. In: Python.org [Internet]. 9 Apr 2024 [cited 23 Apr 2024]. Available: https://www.python.org/
16. TensorFlow. [cited 23 Apr 2024]. Available: https://www.tensorflow.org/
17. Keras: Deep Learning for humans. [cited 23 Apr 2024]. Available: https://keras.io/
18. PyTorch. [cited 23 Apr 2024]. Available: https://pytorch.org/
19. Ayyadevara VK, Reddy Y. Modern Computer Vision with PyTorch: Explore deep learning concepts and implement over 50 real-world image applications. Packt Publishing Ltd; 2020.
20. R Core Team. R: A Language and Environment for Statistical Computing. Vienna, Austria: R Foundation for Statistical Computing; 2024. Available: https://www.R-project.org/
21. R Core Team. R: A Language and Environment for Statistical Computing. Vienna, Austria: R Foundation for Statistical Computing; 2020. Available: https://www.R-project.org/

22. RStudio Team. RStudio: Integrated Development Environment for R. Boston, MA: RStudio, PBC.; 2020. Available: http://www.rstudio.com/
23. Sardá-Espinosa A. Time-Series Clustering in R Using the dtwclust Package. R J. 2019. doi:10.32614/RJ-2019-023
24. Wickham H, Averick M, Bryan J, Chang W, McGowan LD, François R, et al. Welcome to the tidyverse. J Open Source Softw. 2019;4: 1686. doi:10.21105/joss.01686
25. Pebesma E. Simple Features for R: Standardized Support for Spatial Vector Data. R J. 2018;10: 439–446. doi:10.32614/RJ-2018-009
26. Hijmans RJ. terra: Spatial Data Analysis. 2024. Available: https://CRAN.R-project.org/package=terra
27. Pebesma E, Bivand R. Spatial Data Science: With applications in R. London: Chapman and Hall/CRC; 2023. doi:10.1201/9780429459016
28. Tennekes M. tmap: Thematic Maps in R. J Stat Softw. 2018;84: 1–39. doi:10.18637/jss.v084.i06
29. Hijmans RJ. raster: Geographic Data Analysis and Modeling. 2023. Available: https://CRAN.R-project.org/package=raster
30. Yu G. dlstats: Download Stats of R Packages. 2023. Available: https://CRAN.R-project.org/package=dlstats
31. ISO. ISO/IEC 14882:2011 Information technology — Programming languages — C++. Geneva, Switzerland: International Organization for Standardization; 2012. Available: http://www.iso.org/iso/iso_catalogue/catalogue_tc/catalogue_detail.htm?csnumber=50372
32. Eddelbuettel D, Francois R, Allaire JJ, Ushey K, Kou Q, Russell N, et al. Rcpp: Seamless R and C++ Integration. 2024. Available: https://CRAN.R-project.org/package=Rcpp
33. Ushey K, Allaire JJ, Tang Y. reticulate: Interface to "Python." 2024. Available: https://CRAN.R-project.org/package=reticulate
34. Allaire JJ, Chollet F. keras: R Interface to "Keras." 2024. Available: https://CRAN.R-project.org/package=keras
35. Allaire JJ, Tang Y. tensorflow: R Interface to "TensorFlow." 2024. Available: https://CRAN.R-project.org/package=tensorflow
36. Abdullayev T. fastai: Interface to "fastai." 2024. Available: https://CRAN.R-project.org/package=fastai
37. Falbel D, Luraschi J. torch: Tensors and Neural Networks with "GPU" Acceleration. 2023. Available: https://CRAN.R-project.org/package=torch
38. PyTorch C++ API — PyTorch main documentation. [cited 23 Apr 2024]. Available: https://pytorch.org/cppdocs/
39. Maxwell A. geodl example data. 2023. doi:10.6084/m9.figshare.23835165.v2
40. Hester J, Csárdi G, Wickham H, Chang W, Morgan M, Tenenbaum D. remotes: R Package Installation from Remote Repositories, Including "GitHub." 2021. Available: https://CRAN.R-project.org/package=remotes
41. Maxwell AE, Bester MS, Guillen LA, Ramezan CA, Carpinello DJ, Fan Y, et al. Semantic Segmentation Deep Learning for Extracting Surface Mine Extents from Historic Topographic Maps. Remote Sens. 2020;12: 4145. doi:10.3390/rs12244145
42. Prospect- and Mine-Related Features from U.S. Geological Survey 7.5- and 15-Minute Topographic Quadrangle Maps of the United States (ver. 10.0, May 2023) - ScienceBase-Catalog. [cited 27 Apr 2024]. Available: https://www.sciencebase.gov/catalog/item/5a1492c3e4b09fc93dcfd574

43. Maxwell A. topoDL: A deep learning semantic segmentation dataset for the extraction of surface mine extents from historic USGS topographic maps. 2024. doi:10.6084/m9.figshare.25096640.v1
44. Boguszewski A, Batorski D, Ziemba-Jankowska N, Zambrzycka A, Dziedzic T. LandCover. ai: Dataset for Automatic Mapping of Buildings, Woodlands and Water from Aerial Imagery. ArXiv Prepr ArXiv200502264. 2020.
45. QGIS Development Team. QGIS Geographic Information System. QGIS Association; 2024. Available: https://www.qgis.org
46. Falbel D. luz: Higher Level "API" for "torch." 2023. Available: https://CRAN.R-project.org/package=luz
47. Falbel D. torchvision: Models, Datasets and Transformations for Images. 2023. Available: https://CRAN.R-project.org/package=torchvision
48. Sandler M, Howard A, Zhu M, Zhmoginov A, Chen L-C. Mobilenetv2: Inverted residuals and linear bottlenecks. Proceedings of the IEEE conference on computer vision and pattern recognition. 2018. pp. 4510–4520.
49. Wickham H, François R, Henry L, Müller K, Vaughan D. dplyr: A Grammar of Data Manipulation. 2023. Available: https://CRAN.R-project.org/package=dplyr
50. Ilich AR, Misiuk B, Lecours V, Murawski SA. MultiscaleDTM. 2021. doi:10.5281/zenodo.5548338
51. William Revelle. psych: Procedures for Psychological, Psychometric, and Personality Research. Evanston, Illinois: Northwestern University; 2023. Available: https://CRAN.R-project.org/package=psych
52. Maxwell AE, Odom WE, Shobe CM, Doctor DH, Bester MS, Ore T. Exploring the Influence of Input Feature Space on CNN-Based Geomorphic Feature Extraction From Digital Terrain Data. Earth Space Sci. 2023;10: e2023EA002845.
53. Buslaev A, Iglovikov VI, Khvedchenya E, Parinov A, Druzhinin M, Kalinin AA. Albumentations: Fast and Flexible Image Augmentations. Information. 2020;11. doi:10.3390/info11020125
54. Shorten C, Khoshgoftaar TM. A survey on Image Data Augmentation for Deep Learning. J Big Data. 2019;6: 60. doi:10.1186/s40537-019-0197-0
55. Ronneberger O, Fischer P, Brox T. U-net: Convolutional networks for biomedical image segmentation. International Conference on Medical image computing and computer-assisted intervention. Springer; 2015. pp. 234–241.
56. Agarap AF. Deep learning using rectified linear units (relu). ArXiv Prepr ArXiv180308375. 2018.
57. Lu L, Shin Y, Su Y, Karniadakis GE. Dying relu and initialization: Theory and numerical examples. ArXiv Prepr ArXiv190306733. 2019.
58. Wang X, Ren H, Wang A. Smish: A Novel Activation Function for Deep Learning Methods. Electronics. 2022;11: 540. doi:10.3390/electronics11040540
59. He K, Zhang X, Ren S, Sun J. Deep Residual Learning for Image Recognition. ArXiv151203385 Cs. 2015 [cited 2 Jan 2021]. Available: http://arxiv.org/abs/1512.03385
60. Hu J, Shen L, Sun G. Squeeze-and-excitation networks. Proceedings of the IEEE conference on computer vision and pattern recognition. 2018. pp. 7132–7141.
61. Abraham N, Khan NM. A novel Focal Tversky loss function with improved Attention U-Net for lesion segmentation. ArXiv Prepr ArXiv181007842. 2018.

62. Oktay O, Schlemper J, Folgoc LL, Lee M, Heinrich M, Misawa K, et al. Attention u-net: Learning where to look for the pancreas. ArXiv Prepr ArXiv180403999. 2018.
63. Chen L-C, Zhu Y, Papandreou G, Schroff F, Adam H. Encoder-decoder with atrous separable convolution for semantic image segmentation. Proceedings of the European conference on computer vision (ECCV). 2018. pp. 801–818.
64. Chen L-C, Papandreou G, Schroff F, Adam H. Rethinking atrous convolution for semantic image segmentation. ArXiv Prepr ArXiv170605587. 2017.
65. Zhao H, Shi J, Qi X, Wang X, Jia J. Pyramid scene parsing network. Proceedings of the IEEE conference on computer vision and pattern recognition. 2017. pp. 2881–2890.
66. Huang H, Lin L, Tong R, Hu H, Zhang Q, Iwamoto Y, et al. Unet 3+: A full-scale connected unet for medical image segmentation. ICASSP 2020-2020 IEEE international conference on acoustics, speech and signal processing (ICASSP). IEEE; 2020. pp. 1055–1059.
67. Le'Clerc Arrastia J, Heilenkötter N, Otero Baguer D, Hauberg-Lotte L, Boskamp T, Hetzer S, et al. Deeply supervised UNet for semantic segmentation to assist dermatopathological assessment of basal cell carcinoma. J Imaging. 2021;7: 71.
68. Reiß S, Seibold C, Freytag A, Rodner E, Stiefelhagen R. Every annotation counts: Multi-label deep supervision for medical image segmentation. Proceedings of the IEEE/CVF conference on computer vision and pattern recognition. 2021. pp. 9532–9542.
69. Zhou Z, Siddiquee MMR, Tajbakhsh N, Liang J. Unet++: A nested u-net architecture for medical image segmentation. Deep learning in medical image analysis and multimodal learning for clinical decision support. Springer; 2018. pp. 3–11.
70. Howard AG, Zhu M, Chen B, Kalenichenko D, Wang W, Weyand T, et al. Mobilenets: Efficient convolutional neural networks for mobile vision applications. ArXiv Prepr ArXiv170404861. 2017.
71. Keydana S. Deep Learning and Scientific Computing with R Torch. Chapman and Hall/CRC; 2023.
72. Keydana S. Posit AI Blog: Train in R, run on Android: Image segmentation with torch. 2021 [cited 27 Apr 2024]. Available: https://blogs.rstudio.com/tensorflow/posts/2021-10-29-segmentation-torch-android/
73. Deng J, Dong W, Socher R, Li L-J, Li K, Fei-Fei L. Imagenet: A large-scale hierarchical image database. 2009 IEEE conference on computer vision and pattern recognition. Ieee; 2009. pp. 248–255.
74. Li X, Sun X, Meng Y, Liang J, Wu F, Li J. Dice Loss for Data-imbalanced NLP Tasks. ArXiv191102855 Cs. 2020 [cited 14 Jun 2021]. Available: http://arxiv.org/abs/1911.02855
75. Sudre CH, Li W, Vercauteren T, Ourselin S, Cardoso MJ. Generalised Dice overlap as a deep learning loss function for highly unbalanced segmentations. 2017. pp. 240–248. doi:10.1007/978-3-319-67558-9_28
76. Hashemi SR, Salehi SSM, Erdogmus D, Prabhu SP, Warfield SK, Gholipour A. Tversky as a loss function for highly unbalanced image segmentation using 3d fully convolutional deep networks. arXiv preprint arXiv:1803.11078. Jun; 2018.
77. Tharwat A. Classification assessment methods. Appl Comput Inform. 2020;17: 168–192. doi:10.1016/j.aci.2018.08.003
78. Farhadpour S, Warner TA, Maxwell AE. Selecting and Interpreting Multiclass Loss and Accuracy Assessment Metrics for Classifications with Class Imbalance: Guidance and Best Practices. Remote Sens. 2024;16: 533. doi:10.3390/rs16030533

79. Ma J, Chen J, Ng M, Huang R, Li Y, Li C, et al. Loss odyssey in medical image segmentation. Med Image Anal. 2021;71: 102035. doi:10.1016/j.media.2021.102035
80. Lin T-Y, Goyal P, Girshick R, He K, Dollar P. Focal Loss for Dense Object Detection. 2017. pp. 2980–2988. Available: https://openaccess.thecvf.com/content_iccv_2017/html/Lin_Focal_Loss_for_ICCV_2017_paper.html
81. Yeung M, Sala E, Schönlieb C-B, Rundo L. Unified focal loss: Generalising dice and cross entropy-based losses to handle class imbalanced medical image segmentation. Comput Med Imaging Graph. 2022;95: 102026.
82. Jadon S. A survey of loss functions for semantic segmentation. 2020 IEEE conference on computational intelligence in bioinformatics and computational biology (CIBCB). IEEE; 2020. pp. 1–7.
83. Gowda T, You W, Lignos C, May J. Macro-average: rare types are important too. ArXiv Prepr ArXiv210405700. 2021.
84. Grandini M, Bagli E, Visani G. Metrics for multi-class classification: an overview. ArXiv Prepr ArXiv200805756. 2020.
85. Maxwell AE, Warner TA, Guillén LA. Accuracy Assessment in Convolutional Neural Network-Based Deep Learning Remote Sensing Studies—Part 1: Literature Review. Remote Sens. 2021;13: 2450. doi:10.3390/rs13132450
86. Maxwell AE, Warner TA, Guillén LA. Accuracy Assessment in Convolutional Neural Network-Based Deep Learning Remote Sensing Studies—Part 2: Recommendations and Best Practices. Remote Sens. 2021;13: 2591. doi:10.3390/rs13132591
87. LeCun Y, Bengio Y, Hinton G. Deep learning. nature. 2015;521: 436–444.
88. LeCun Y, Bottou L, Bengio Y, Haffner P. Gradient-based learning applied to document recognition. Proc IEEE. 1998;86: 2278–2324.
89. LeCun Y, Boser B, Denker JS, Henderson D, Howard RE, Hubbard W, et al. Backpropagation applied to handwritten zip code recognition. Neural Comput. 1989;1: 541–551.
90. Duchi J, Hazan E, Singer Y. Adaptive subgradient methods for online learning and stochastic optimization. J Mach Learn Res. 2011;12.
91. Zeiler MD. Adadelta: an adaptive learning rate method. ArXiv Prepr ArXiv12125701. 2012.
92. Tieleman T, Hinton G, others. Lecture 6.5-rmsprop: Divide the gradient by a running average of its recent magnitude. COURSERA Neural Netw Mach Learn. 2012;4: 26–31.
93. Kingma DP, Ba J. Adam: A method for stochastic optimization. ArXiv Prepr ArXiv14126980. 2014.
94. Loshchilov I, Hutter F. Decoupled weight decay regularization. ArXiv Prepr ArXiv171105101. 2017.
95. Smith LN. Cyclical Learning Rates for Training Neural Networks. 2017 IEEE Winter Conference on Applications of Computer Vision (WACV). 2017. pp. 464–472. doi:10.1109/WACV.2017.58
96. Smith LN, Topin N. Super-convergence: Very fast training of neural networks using large learning rates. Artificial Intelligence and Machine Learning for Multi-Domain Operations Applications. International Society for Optics and Photonics; 2019. p. 1100612.
97. Congalton RG, Green K. Assessing the accuracy of remotely sensed data: principles and practices. CRC press; 2019.

98. Foody GM. Status of land cover classification accuracy assessment. Remote Sens Environ. 2002;80: 185–201.
99. Stehman SV, Czaplewski RL. Design and Analysis for Thematic Map Accuracy Assessment: Fundamental Principles. Remote Sens Environ. 1998;64: 331–344. doi:10.1016/S0034-4257(98)00010-8
100. Stehman SV, Foody GM. Key issues in rigorous accuracy assessment of land cover products. Remote Sens Environ. 2019;231: 111199. doi:10.1016/j.rse.2019.05.018
101. Foody GM. Explaining the unsuitability of the kappa coefficient in the assessment and comparison of the accuracy of thematic maps obtained by image classification. Remote Sens Environ. 2020;239: 111630.
102. Pontius Jr RG, Millones M. Death to Kappa: birth of quantity disagreement and allocation disagreement for accuracy assessment. Int J Remote Sens. 2011;32: 4407–4429.
103. Stehman SV, Foody GM, others. Accuracy assessment. The SAGE handbook of remote sensing. Sage London; 2009. pp. 297–309.
104. Bommasani R, Hudson DA, Adeli E, Altman R, Arora S, von Arx S, et al. On the opportunities and risks of foundation models. ArXiv Prepr ArXiv210807258. 2021.
105. Kirillov A, Mintun E, Ravi N, Mao H, Rolland C, Gustafson L, et al. Segment anything. Proceedings of the IEEE/CVF International Conference on Computer Vision. 2023. pp. 4015–4026.
106. Stewart AJ, Robinson C, Corley IA, Ortiz A, Ferres JML, Banerjee A. TorchGeo: Deep Learning With Geospatial Data. 2022.
107. Chen L-C, Papandreou G, Kokkinos I, Murphy K, Yuille AL. Deeplab: Semantic image segmentation with deep convolutional nets, atrous convolution, and fully connected crfs. IEEE Trans Pattern Anal Mach Intell. 2017;40: 834–848.
108. Yakubovskiy P. Segmentation Models Pytorch. GitHub repository. GitHub; 2020. Available: https://github.com/qubvel/segmentation_models.pytorch
109. Xie E, Wang W, Yu Z, Anandkumar A, Alvarez JM, Luo P. SegFormer: Simple and efficient design for semantic segmentation with transformers. Adv Neural Inf Process Syst. 2021;34: 12077–12090.